Topological magnetization jumps in a confined chiral soliton lattice

Jun-ichiro Kishine
Division of Natural and Environmental Sciences, The Open University of Japan, Chiba, 261-8586, Japan

I. G. Bostrem, A. S. Ovchinnikov, and Vl. E. Sinitsyn
Institute of Natural Sciences, Ural Federal University, Ekaterinburg, 620083, Russia
(Received 14 September 2013; revised manuscript received 24 December 2013; published 22 January 2014)

We demonstrate that a finite-size chiral soliton lattice formed in a chiral helimagnet with fixed boundary conditions exhibits magnetization jumps in a response to the magnetic field applied perpendicular to the chiral axis. The imposed boundary conditions lead to confinement of topological charges and quantized spatial periods of the soliton lattice. Building an envelope of the ground-state energies belonging to different topological sectors, we find the magnetization jumps related with the level crossing. After numerically establishing the quantization condition, we also develop a field-theoretical model to support the numerical results.

DOI: 10.1103/PhysRevB.89.014419 PACS number(s): 75.75.−c, 41.20.Gz, 75.25.−j, 81.05.Xj

I. INTRODUCTION

In recent years, chiral helimagnets, where antisymmetric Dzyaloshinskii-Moriya (DM) interactions induce long-range modulations of magnetic order, became a subject of active experimental and theoretical investigations. The interest is foremost aroused by an opportunity to observe stable magnetic topological structures. They can be realized either as whirls of magnetization (the so-called skyrmions) observed, for example, in MnSi [1], $Fe_{1-x}Co_xSi$ [2], and Cu_2OSeO_3 [3], or as a spiral helimagnetic order, which can be deformed by an external magnetic field. In particularly, the long-standing prediction by Dzyaloshinskii was experimentally verified in the hexagonal chiral magnet $Cr_{1/3}NbS_2$ by using Lorenz microscopy and small-angle electron diffraction [4]. It claims that the magnetic field applied perpendicular to the helical axis stabilizes a topological ground state of the chiral helimagnet called magnetic soliton lattice [5]. The chiral soliton lattice (CSL) presents a periodic array of 2π domain walls (kinks) and their number coincides with the topological one.

One aspect of the studies of the chiral helimgnets is related with the use of their non-trivial magnetic patterns in modern spintronic devices [6]. For instance, it has been demonstrated that a control and detection of a motion of the skyrmions by weak electric currents may be important route towards spintronic applications [7]. Manipulation of the chiral magnetic spiral with the magnetic field and/or the electric current has been theoretically discussed in Refs. [8–10]. The noticable negative magnetoresistance protected by chirality have been recently observed in $Cr_{1/3}NbS_2$ in a wide range of temperature below incommensurate-commensurate phase transition [11].

In practice, to realize storage technologies or spintronic devices based on the chiral magnets, it is essential to understand their physics for finite-size samples or systems with a reduced dimensionality. For instance, the modeling of skyrmion dynamics in constricted geometries have been carried out in Ref. [12]. There are experimental evidences that the epitaxial induced strain in the thin films of MnSi results in an appearance of states (i.e., skyrmions) that are metastable or absent in the bulk MnSi [13]. Another remarkable feature found in magnetometry measurements in MnSi thin films is the sudden jumps in magnetization seen in the field-induced unwinding of the confined helicoid [14]. Apparently, the discrete change of the helicoidal structure provides a promising functionality for spintronic devices and a theoretical treatment of the effect is highly required.

The problem is not as simple as it might seem at first glance. Obviously, the finite-size solution for magnetization with imposed fixed boundary conditions (BC) changes substantially as compared with the bulk one, because the confined chiral solitons repel each other and we expect topological quantization of the soliton lattice period to accommodate an integer number of solitons over a finite system. However, any naive attack of the isoperimetric variational problem by standards methods, i.e., a seeking of conditional extremum, faces serious difficulties. Indeed, the linear Lifshitz invariant coming from the DM term and fixing the topological charge takes the form of a total derivative and, as a result, the BC cannot be incorporated into the variational scheme. In this context, we note that in Ref. [14] the discrete jumps of magnetization were proposed based on the variational analysis by taking account of finite sample thickness with free boundary conditions.

In this paper, to clarify the effects of the boundary pinning on the bulk magnetization in an explicit manner, we perform an unbiased numerical analysis of the lattice model and discuss the ground state spin configurations with an imposed BC. Based on the numerically justified quantization condition for the spatial periods of the CSL, a level-crossing scheme of the ground state energies is formulated and the resultant magnetization jumps are naturally explained.

The paper is organized as follows. In Sec. II, the lattice model and the details of the routines used in the numerical calculations are introduced. In Sec. III, we present the numerical results, which justifies the topological quantization condition. The analytical model supporting the numerical findings is developed in Sec. IV. Finally, we make concluding remarks in Sec. V.

II. FORMULATION

We consider a *finite-size* chain of the classical chiral helimagnet (CHM) with the fixed BC on both ends, as shown in

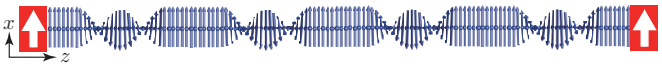

FIG. 1. (Color online) A finite-size chiral soliton lattice considered here, where spins on both ends are fixed in a parallel manner. The whole system is put under the magnetic field applied perpendicular to the helical axis.

Fig. 1. A classical spin at the ith site, $\boldsymbol{S}_i = S(\cos\varphi_i, \sin\varphi_i, 0)$, is parametrized by the angle φ_i obeying the BC:

$$\varphi_0 = 0 \quad \text{and} \quad \varphi_N = -2\pi n, \tag{1}$$

where $i = 0$ and N correspond to sites at the edges. A topological number n specifies the whole number of solitons accommodated in the system and determined by the winding numbers of the homotopy group $\pi_1(S_1)$. This kind of BC may be realized, for example, by attaching ferromagnetic slabs on both ends of the chiral helimagnet. The total energy of the system is described by an effective one-dimensional Hamiltonian,

$$H/JS^2 = -\sum_{i=0}^{N-1}\cos(\varphi_{i+1} - \varphi_i) + D_z/J\sum_{i=0}^{N-1}\sin(\varphi_{i+1} - \varphi_i) - h\sum_{i=0}^{N}\cos\varphi_i, \tag{2}$$

where $J > 0$ is the nearest-neighbor ferromagnetic exchange interaction and D_z is the mono-axial Dzyaloshinskii-Moriya interaction along a certain crystallographic chiral axis (taken here as the z axis). The magnetic field H_x is applied perpendicular to the chiral axis. The dimensionless field strength is $h \equiv g\mu_B H_x/JS$, where g is the electron g factor and μ_B is the Bohr magneton. In the case of an infinite system with the free BC, the zero-field ground state is the CHM with the spiral modulation wave number $Q_0 = \arctan(D_z/J)$. In the numerical calculations below, we took $D_z/J = 0.16$ corresponding to the value observed in $Cr_{1/3}NbS_2$ [4].

The lattice version of Landau-Lifshitz equations results in equation for the variables φ_i (see Appendix A):

$$0 = \gamma\sin(\varphi_i - \varphi_{i-1} + \delta) - \gamma\sin(\varphi_{i+1} - \varphi_i + \delta) + h\sin\varphi_i, \tag{3}$$

where $\delta = \arctan(D_z/J)$ and $\gamma = \sqrt{1 + D_z^2/J^2}$. In order to perform numerical computations, it is convenient to split Eq. (3) to a form convenient for an iterative routine (see Ref. [8]):

$$\sin\varphi_i = (\gamma\sin(\varphi_{i+1} + \delta) + \gamma\sin(\varphi_{i-1} - \delta)) \times [\gamma^2(\sin(\varphi_{i+1} + \delta) + \sin(\varphi_{i-1} - \delta))^2 + (\gamma\cos(\varphi_{i-1} - \delta) + \gamma\cos(\varphi_{i+1} + \delta) + h)^2]^{-1/2}, \tag{4}$$

$$\cos\varphi_i = (\gamma\cos(\varphi_{i-1} - \delta) + \gamma\cos(\varphi_{i+1} + \delta) + h) \times [\gamma^2(\sin(\varphi_{i+1} + \delta) + \sin(\varphi_{i-1} - \delta))^2 + (\gamma\cos(\varphi_{i-1} - \delta) + \gamma\cos(\varphi_{i+1} + \delta) + h)^2]^{-1/2}. \tag{5}$$

The static spin configuration is found by using the iteration scheme. The numerical algorithm starts by initializing the values of spin variables. Scanning linearly the chain, the spin variable at each site gets updated according to Eqs. (4) and (5), being reset along the net field due partly to some unchanged neighbors and some that have already been repointed. The iterations stop if the sum $\sqrt{\sum_{i=0}^{N}(\varphi_i^{(k)} - \varphi_i^{(k-1)})^2}$ taken over the chain on the kth step is less than tolerance 10^{-8}.

III. NUMERICAL RESULTS

By using the numerical scheme set out above, we computed the ground state energy, $E_{\min}/JS^2$, associated with the Hamiltonian (2) for the systems consisting of $N + 1 = 211$, 411, and 811 sites. In our calculations, the trying starting configurations were taken as $\varphi_i = -2\pi ni/N$ that is compatible with the imposed boundary conditions (1). The topological number n is firstly fixed and we search for the minimum energy as a function of h. In Fig. 2, the results for the case of 411 sites are shown. In the case of $h = 0$, we found that the system relaxes to the CHM state with the maximal topological number $n_{\max} = [NQ_0/2\pi]$. In the current case, $D_z/J = 0.16$ and $N = 410$, thus, we have $n_{\max} = [10.353] = 10$. As h increases and the soliton lattice starts to form, the topological number for the stable ground state exhibits cascade transitions to $n = n_{\max} - 1, n_{\max} - 2, \ldots, 1$ at the critical field strengths where the energy levels cross each other. The envelope of the ground-state energies provides a series of phase transitions from one topological sector to another with smaller n. At higher fields, the energy levels are distributed so dense that the energy crossing points almost merge and become hardly resolved.

In Fig. 3, we show the coordinate behavior of φ_i corresponding to the ground states of the different topological sectors. It is clearly seen that for $h = 0$ ($n = n_{\max}$), the system adjusts itself to the BC by matching the spatial period to the smallest value close to the bulk period. A larger value, $n_{\max} + 1$, is disfavored because of the energy costs associated with the ferromagnetic exchange.

In each topological sector, the number n is found to be conserved and the kinks form regular lattice structure. In Fig. 4(a), we show h dependence of the lattice period ℓ for

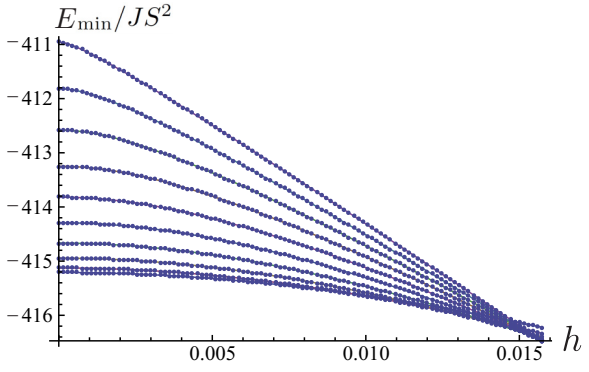

FIG. 2. (Color online) Magnetic field dependence of minimum energies, $E_{\min}/JS^2$, belonging to different topological sectors with $n = 10, 9, \ldots, 1$ from the bottom to the top, for the case of $D_z/J = 0.16$ and $N = 410$.

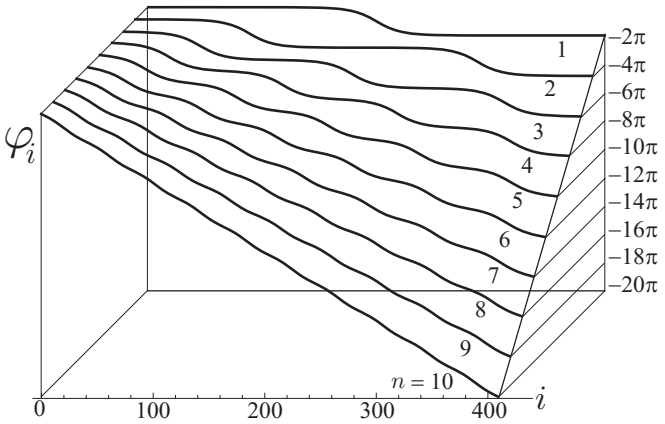

FIG. 3. Spatial modulation of the phase angle φ_i (measured in 2π units) corresponding to the minimum energy states at typical magnitude of h belonging to different topological sectors $n = 10,9,\ldots,1$, for the case of $D_z/J = 0.16$ and $N = 410$.

$N = 810$ ($n_{\max} = 20$). We see that the period jumps at the energy-crossing points and exhibits a steplike behavior. Each step gives the quantized period

$$\ell_n = N/n. \tag{6}$$

This result is the most essential finding of the numerical analysis and it is out of reach of the standard variational analysis based on the continuum version of the lattice Hamiltonian (2). It is seen that ℓ_n is kept *constant* irrespective of h within each topological sector. In Fig. 4(a), we also show the analytical

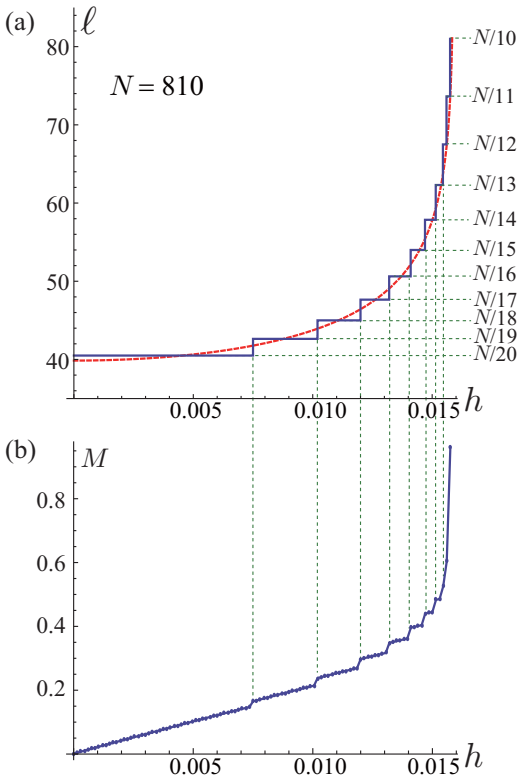

FIG. 4. (Color online) (a) Numerical (solid line) and analytical (dotted line) field dependencies of the spatial period and (b) magnetization curve, for the case of $D_z/J = 0.16$ $N = 810$.

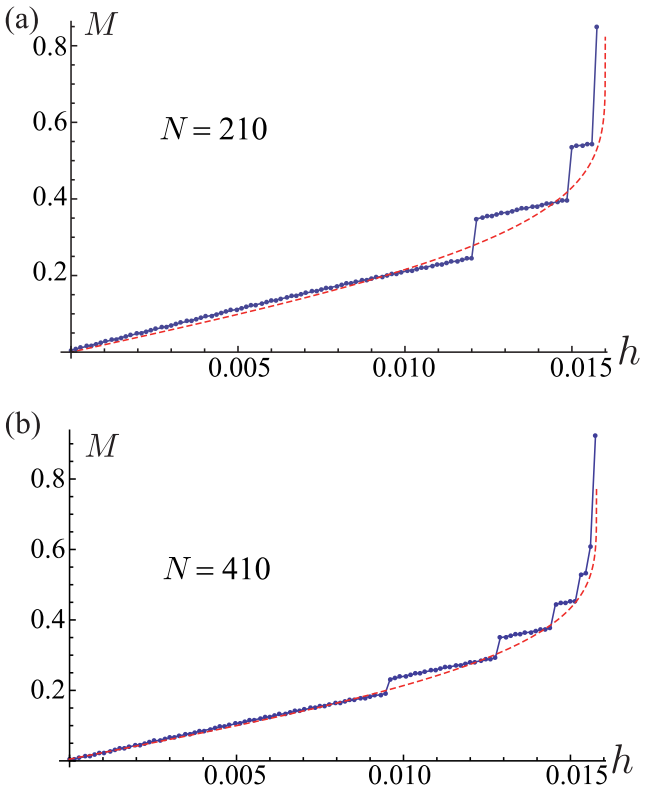

FIG. 5. (Color online) Magnetization curves for (a) $N = 210$ and (b) 410. Analytical magnetization curve for the infinite system is also shown by the dotted lines.

result for the period of the infinite system, which is expressed by Eq. (9) given below.

The magnetization per site is computed as $M = \frac{1}{N+1}\sum_{i=0}^{N}\cos\varphi_i$. In Fig. 4(b), we show the h dependence of M. In each topological sector, M increases almost linearly as a function of h and exhibits jumps at the energy-crossing point. In Fig. 5, we show the magnetization for the cases of 211 and 411 sites. It is seen that for a larger system the magnetization curve becomes more smooth and approaches the bulk magnetization [15]. This change describes quantum-to-classical crossover in the confined soliton system.

IV. AN ANALYTICAL MODEL OF THE QUANTIZED PERIOD

The found numerical results for quantization of the CSL period can be reproduced by a slight modification of the variational analysis of the continuum version of the Hamiltonian (2). This approach is relevant because of the slowly varying nature of the spin variables, $\boldsymbol{S}(z) = \sum_i \boldsymbol{S}_i\delta(z - z_i) \equiv S\boldsymbol{n}(z)$, parametrized by the unit vector field $\boldsymbol{n}(z) = (\cos\varphi(z), \sin\varphi(z), 0)$. The transformation converts (2) into the form, which is nothing but the Pokrovsky-Talapov (PT) model [16],

$$\mathcal{H}/JS^2 = \int_0^N dz\left[\frac{1}{2}(\partial_z\varphi)^2 + Q_0\partial_z\varphi - h\cos\varphi\right], \tag{7}$$

where the atomic lattice constant is set to unity. Hereinafter, N plays a role of the length of the system, and $Q_0 = D_z/J$. A

conventional variational analysis gives the CSL configuration,

$$\varphi(z) = -\pi - 2\mathrm{am}\left(\tfrac{\sqrt{h}}{\kappa} z\right), \tag{8}$$

where am is the Jacobi's amplitude function with the elliptic modulus κ ($0 \leqslant \kappa < 1$). The period of CSL is given by

$$\ell = 2\kappa K(\kappa)/\sqrt{h}, \tag{9}$$

where $K(\kappa)$ is the complete elliptic integral of the first kind. In the *bulk* case, following the recipe presented by Dzyaloshinskii [5] and de Gennes [17], one should minimize the total energy with respect to the elliptic modulus κ that yields $\kappa = 4E(\kappa)\sqrt{h}/(\pi Q_0)$, where $E(\kappa)$ is the complete elliptic integral of the second kind.

However, in the *finite-size* system considered here, the BC prevents us from searching the global energy minimum as a function of κ. Instead, the quantization condition (6) should be employed:

$$2\kappa_n K(\kappa_n)/\sqrt{h} = N/n, \tag{10}$$

which determines the discrete elliptic modulus κ_n as a function of h. It should be stressed again that this condition is beyond the variational scheme, because it is impossible to obtain the condition (6) via any variational procedure for the continuum model (7), where the linear Lifshitz invariant $Q_0\partial_z\varphi$ gives no contribution to the variational equation. In this context, we mention that the theoretical analysis for MnSi films given in Ref. [14] for free boundary conditions derives the parameter κ from minimizing of the energy density averaged over the layer thickness, and the κ varies continuously with the magnetic field.

By taking the condition (10), we use κ_n in Eq. (8) to compute the continuum energy,

$$\frac{\mathcal{H}}{JS^2} = \frac{4n\sqrt{h}}{\kappa_n}\left[2E(\kappa_n) - \left(1 - \frac{\kappa_n^2}{2}\right)K(\kappa_n)\right] - 2\pi Q_0 n. \tag{11}$$

In Fig. 6(a), we show the h dependence of $\mathcal{H}$ for different topological sectors (we set $N = 410$). The result is qualitatively well consistent with the numerical one [we also present an approximate analysis for a weak field limit in Appendix B]. From Eq. (11), the competition between the commensurability (exchange and Zeeman) and incommensurability (DM) energies is elucidated. The exchange and Zeeman terms are combined to give the first term in the r.h.s., which tends to increase the commensurate domain and, as a function of h, decreases more rapidly as the topological number $n$decreases. On the other hand, the DM term gives the n-dependent intercept and favours larger topological numbers. We emphasize that the first term is a part of the *sine-Gordon (SG) model* (with $Q_0 = 0$), whereas the second term depends explicitly on Q_0. A detailed discussion of differences between the SG model and the PT model with the finite Q_0 is given in Ref. [18] within the renormalization-group analysis.

By using Eq. (8), the magnetization is merely computed as

$$M_n = \frac{1}{N}\int_0^N dz\, \cos\varphi = -1 + \frac{2}{\kappa_n^2} - \frac{2E(\kappa_n)}{\kappa_n^2 K(\kappa_n)}. \tag{12}$$

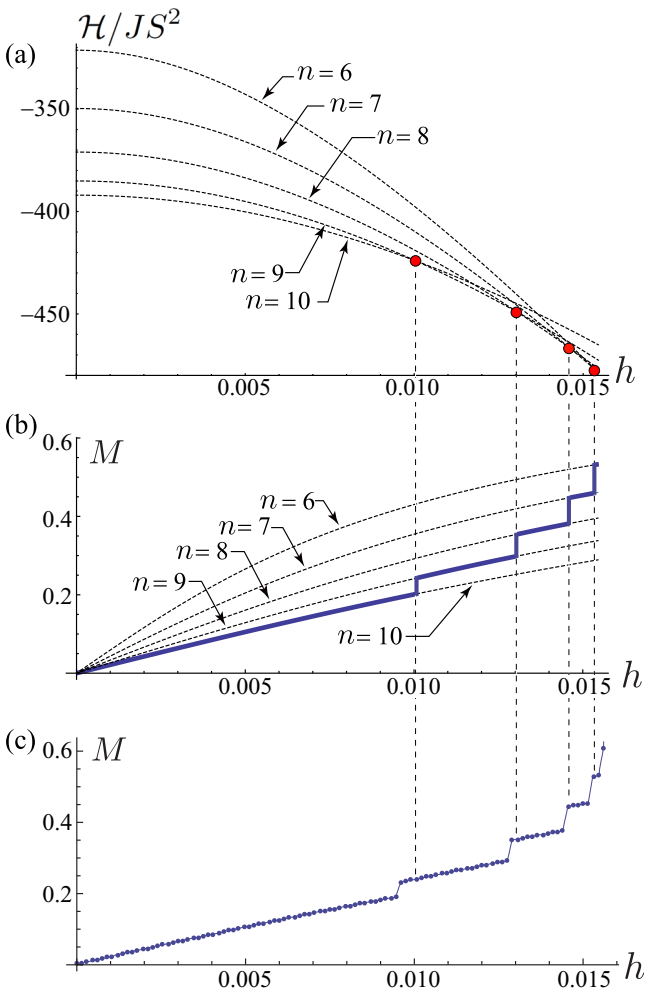

FIG. 6. (Color online) (a) Energy given by Eq. (11) as function of h for $n = 10,9,8,7,6$. Energy crossing points are indicated by circles. (b) Magnetization curves given by Eq. (12). Figure 5(b) is reproduced in (c) to make a comparison between the analytic and numerical results.

In Fig. 6(b), we show the magnetization curves for $n =$ 6–10. As h increases, the ground state magnetization curve, indicated by the thick line, jumps at a critical field h_n from $(n+1)$ sector to n sector. We repeat Fig. 5(b) as Fig. 6(c) to compare the analytical result with the numerical one. Although in the continuum approximation the terms containing $(\partial_z\varphi)^m$ ($m \geqslant 3$) are omitted, analytical results are qualitatively consistent with numerical results based on the lattice model. With changing h inside each topological sector, the shape of the texture does not exhibit any visible change and abruptly jumps to the next topological sector at critical fields h_n.

We note an essential different role of the fixed BC in formation of the magnetization jumps in our system and in finite-size Heisenberg spin chains. In the last case, steps in a magnetization curve arise from the discretness of the energy spectrum. A fixing of the boundary spins lifts only the SU(2) degeneracy but the spectrum remains untouched. In the case of the CHM, the energy states are indexed by the parameter κ, which varies continuously with the magnetic

field for the infinite system or for the finite system with free boundary conditions. By fixing spins at the edges, the spectrum changes drastically and becomes discrete with values determined by κ_n, i.e., by a number of periods of the CSL.

V. CONCLUDING REMARKS

In this paper, we theoretically demonstrated a phenomena of topological quantization of the soliton lattice period in a finite-size chiral helimagnet with fixed boundary conditions. We first presented the numerical analysis to seek for the ground state of the lattice version of the model. An essential finding is that the spatial period of the solitons is quantized to $L_n = N/n$ (where N is the system size and $n = 1,2,\ldots,N$). The quantum number exhibits abrupt jumps to the next one as the fields increase. This phenomena is a direct consequence of the soliton-confinement into the finite size system. As a consequence of this effect, the magnetization curves exhibit abrupt jumps at given values of the field corresponding to the transition from one quantum number to another. To describe the numerical results from analytical viewpoints, we considered a continuum version of the model under the quantization condition and obtained the consistent results. We stress *our model analysis is justified only after the quantization condition was numerically confirmed*.

As comments, we discuss a peculiarity of the suggested mechanism as compared with known phenomena of magnetization jumps. Quantization of physical quantity under changing magnetic field takes place in a wide class of quantum phenomena such as Josephson effect [19], quantum Hall effect [20], quantized flux in superconductors [21], and magnetization plateaus in spin chains [22]. Another example is the well-known classical Barkhausen effect [23] caused by an irreversible magnetic domain wall motion by breaking it away from pinning sites. In comparison with these phenomena, magnetization jumps presented in this study have their origin in the repulsive interaction between the topological charges protected by crystal chirality. By confining the topological charges in the finite system, the spatial period of the CSL gets quantized that provides the magnetization jumps.

Finally, we point out that the quantization scheme developed in the paper may be applied to a wider class of phenomena described by the PT model, which universally describes incommensurate-to-commensurate phase transitions in condensed matters. Especially, the problem of vortex depinning in artificial vortex-flow channels of finite length in type-II superconducting films should be singled out. Previously, it has been analyzed within the PT model and a crucial role of the sample boundaries on the depinning transition has been demonstrated [24].

ACKNOWLEDGMENTS

J.K. and A.S.O. acknowledge stimulating discussions with Y. Togawa. This work was supported by JSPS KAKENHI Grant Nos. 25287087, 24108506, and 25220803. The research was also carried out in terms of Ural Federal University development program with the financial support of young scientists. Vl.E.S. acknowledges RFBR Grant No. 12-02-31565 mol_a.

APPENDIX A: EQUATIONS OF MOTION OF A CHIRAL HELIMAGNET

Monoaxial CHM is described by an effective one-dimensional Hamiltonian,

$$\mathcal{H} = -J\sum_i \boldsymbol{S}_i\cdot\boldsymbol{S}_{i+1} + D_z\sum_i [\boldsymbol{S}_i\times\boldsymbol{S}_{i+1}]_z - g\mu_B H_x\sum_i S_i^x, \tag{A1}$$

where $\mathbf{S}_i = S\boldsymbol{n}_i$ is the local spin moment at the site i, and the parametrization through the unit field $\boldsymbol{n}_i = (\sin\theta_i\cos\varphi_i, \sin\theta_i\sin\varphi_i, \cos\theta_i)$ with the polar angles θ_i and φ_i is used.

The Euler-Lagrange equations of motion are then given by

$$\hbar S\sin\theta_i\,\partial_t\theta_i = \frac{\delta\mathcal{H}}{\delta\varphi_i}, \qquad \hbar S\sin\theta_i\,\partial_t\varphi_i = -\frac{\delta\mathcal{H}}{\delta\theta_i}, \tag{A2}$$

that leads to the system in the lattice form:

$$\frac{d\theta_i}{d\tau} = \sqrt{1+\frac{D^2}{J^2}}\sin\theta_{i-1}\sin(\varphi_i-\varphi_{i-1}+\delta) - \sqrt{1+\frac{D^2}{J^2}}\sin\theta_{i+1}\sin(\varphi_{i+1}-\varphi_i+\delta) + h\sin\varphi_i, \tag{A3a}$$

$$\frac{d\varphi_i}{d\tau} = -(\cos\theta_{i+1}+\cos\theta_{i-1}) + \sqrt{1+\frac{D^2}{J^2}}\cot\theta_i\sin\theta_{i-1}\cos(\varphi_i-\varphi_{i-1}+\delta) + \sqrt{1+\frac{D^2}{J^2}}\cot\theta_i\sin\theta_{i+1}\cos(\varphi_{i+1}-\varphi_i+\delta) + h\cot\theta_i\cos\varphi_i, \tag{A3b}$$

where $\tau = t/\tau_0$ with $\tau_0 = \hbar/JS$.

For the static spin configurations considered in the paper it is supposed that $\theta_i = \pi/2$, which reduces the system to Eq. (3) and the Hamiltonian (A1) modifies into the form given by Eq. (2).

APPENDIX B: MAGNETIZATION FOR A WEAK FIELD LIMIT

The magnetization jumps presented in this paper can be analytically described based on the formulas (10), (11), and (12). We first specify a topological sector n. Second, we determine κ_n as a function of h by using Eq. (10). Then, we determine the energy as a function of h by using Eq. (11). Finally, we compute the magnetization as a function of h by using Eq. (12). The appearance of the jumps is a direct consequence of the energy crossing [see Fig. 6(a)]. To grapple with the analytic structure of the crossing, it may be useful to see the field dependence of the energy for a weak field

limit, i.e., $h \ll 1$. This limit corresponds to the condition, $\kappa_n \ll 1$, and then Eq. (10) gives $\kappa \simeq \frac{N}{\pi n}\sqrt{h}$. Using this relation in the series expansion formulas for $K(\kappa)$ and $E(\kappa)$, we obtain

$$K \simeq \frac{\pi}{2} + \frac{1}{8\pi}\frac{N^2}{n^2}h + \frac{9}{128\pi^3}\frac{N^4}{n^4}h^2 + \mathcal{O}(h^3), \quad \text{(B4)}$$

$$E \simeq \frac{\pi}{2} - \frac{1}{8\pi}\frac{N^2}{n^2}h - \frac{3}{128\pi^3}\frac{N^4}{n^4}h^2 + \mathcal{O}(h^3). \quad \text{(B5)}$$

Plugging these expressions into Eq. (11) gives

$$\frac{\mathcal{H}}{JS^2} = 2\frac{\pi^2}{N}n^2 - \frac{1}{2}Nh\left(1 + \frac{7}{16\pi^2}\frac{N^2}{n^2}h\right) - 2\pi Q_0 n. \quad \text{(B6)}$$

We see that the first term comes from the ferromagnetic exchange which causes an energy cost due to making solitons. The second and third terms arise from the Zeeman interaction. The fourth term is the Lifshitz invariant topological term. From this formula, it is clearly seen that the energy is a downward-convex quadratic function of h with n-dependent intercepts.

[1] S. Mühlbauer, B. Binz, F. Jonietz, C. Pfleiderer, A. Rosch, A. Neuebauer, R. Georgii, and P. Boni, Science **323**, 915 (2009).

[2] P. Milde, O. Köhler, J. Seider, L. M. Eng, A. Bauer, A. Chacou, J. Kindervater, S. Mühlbauer, C. Pfleiderer, S. Buhranndt, C. Schütte, and A. Garst, Science **340**, 1076 (2013).

[3] S. Seki, X. Z. Yu, S. Ishiwata, and Y. Tokura, Science **336**, 198 (2012).

[4] Y. Togawa, T. Koyama, K. Takayanagi, S. Mori, Y. Kousaka, J. Akimitsu, S. Nishihara, K. Inoue, A. S. Ovchinnikov, and J. Kishine, Phys. Rev. Lett. **108**, 107202 (2012).

[5] I. E. Dzyaloshinskii, Zh. Eksp. Teor. Fiz. **46**, 1420 (1964) [Sov. Phys. JETP **19**, 960 (1964)]; Zh. Eksp. Teor. Fiz. **47**, 992 (1964) [Sov. Phys. JETP **20**, 665 (1965)].

[6] N. S. Kiselev, A. N. Bogdanov, R. Schäffer, and U. Rössler, J. Phys. D: Appl. Phys. **44**, 392001 (2011).

[7] T. Shulz, R. Ritz, A. Bauer, M. Halder, M. Wagner, C. Franz, C. Pfleiderer, K. Everschor, M. Garst, and A. Rosch, Nat. Phys. **8**, 301 (2012).

[8] J.-i. Kishine, I. G. Bostrem, A. S. Ovchinnikov, and Vl. E. Sinitsyn, Phys. Rev. B **86**, 214426 (2012).

[9] J.-i. Kishine, A. S. Ovchinnikov, and I. V. Proskurin, Phys. Rev. B **82**, 064407 (2010).

[10] J.-i. Kishine, I. V. Proskurin, and A. S. Ovchinnikov, Phys. Rev. Lett. **107**, 017205 (2011).

[11] Y. Togawa, Y. Kousaka, S. Nishihara, K. Inoue, J. Akimitsu, A. S. Ovchinnikov, and J. Kishine, Phys. Rev. Lett. **111**, 197204 (2013).

[12] J. Iwasaki, M. Mochizuki, and N. Nagaosa, Nat. Nanotechnol. **8**, 742 (2013).

[13] M. N. Wilson, E. A. Karhu, A. S. Quigley, U. K. Rössler, A. B. Butenko, A. N. Bogdanov, M. D. Robertson, and T. L. Monchesky, Phys. Rev. B **86**, 144420 (2012).

[14] M. N. Wilson, E. A. Karhu, D. P. Lake, A. S. Quigley, S. Meynell, A. N. Bogdanov, H. Fritzsche, U. K. Rößler, and T. L. Monchesky, Phys. Rev. B **88**, 214420 (2013).

[15] J. Kishine, K. Inoue, and Y. Yoshida, Prog. Theoret. Phys., Supplement **159**, 82 (2005).

[16] V. L. Pokrovsky and A. L. Talapov, Phys. Rev. Lett. **42**, 65 (1979).

[17] P. G. de Gennes, Solid State Commun. **6**, 163 (1968).

[18] A. Lazarides, O. Tieleman, and C. Morais Smith, Phys. Rev. B **80**, 245418 (2009). In general, the SG model exhibits Kosterlitz-Thouless (KT)-type transition, when the PT model gives both the KT transition and the IC-C phase transition.

[19] S. Shapiro, Phys. Rev. Lett. **11**, 80 (1963); J. M. Rowell, *ibid.* **11**, 200 (1963); A. H. Dayem and J. J. Wiegand, Phys. Rev. **155**, 419 (1967).

[20] R. B. Laughlin, Phys. Rev. B **23**, 5632 (1981); D. J. Thouless, M. Kohmoto, M. P. Nightingale, and M. den Nijs, Phys. Rev. Lett. **49**, 405 (1982).

[21] B. S. Deaver and W. M. Fairbank, Phys. Rev. Lett. **7**, 43 (1961); R. Doll and M. Näbauer, *ibid.* **7**, 51 (1961).

[22] M. Oshikawa, M. Yamanaka, and I. Affleck, Phys. Rev. Lett. **78**, 1984 (1997).

[23] H. Barkhausen, Z. Phys. **20**, 401 (1919).

[24] T. Dröse, R. Besseling, P. Kes, and C. Morais Smith, Phys. Rev. B **67**, 064508 (2003).